nzsee
NEW ZEALAND SOCIETY FOR EARTHQUAKE ENGINEERING

Performance of seismically isolated high-speed railway bridges against near-fault ground motions

Ravi Jangid & Manish Kumar
Indian Institute of Technology Bombay, Mumbai, India.

ABSTRACT

The first high-speed rail (HSR) corridor in India, built on viaducts and bridge structures, is currently under construction between Mumbai and Ahmedabad. This corridor passes through seismic Zone III, whereas future corridors are planned to be constructed in Zones IV and V of the Indian seismic codes. It is challenging and uneconomical to achieve the seismic performance goals of HSR bridges through conventional seismic design measures in higher seismic zones. Seismic isolation technology, which has been successfully deployed for seismic safety of highway and railway bridges in the past, may also be utilized for HSR bridges. However, the HSR bridges have stringent serviceability requirements through limits on deck end rotations (in-plane and out-of-plane), mid-span deflection (in-plane), deck acceleration, and rail stresses. These response parameters in seismically isolated HSR bridges are sensitive to near-fault ground shaking with large amplitude velocity pulses and the presence of low-frequency excitations.

This paper investigates the seismic response of a seismically isolated three-span continuous HSR bridge subject to near-fault ground shaking. A three-dimensional nonlinear finite element model, incorporating track-structure interaction, is developed to compare the seismic performance of the seismically isolated bridge to three ground motions such as far-fault, near-fault pulse type, and near-fault non-pulse type. The ground motions were scaled to the target spectra using amplitude and spectrum matching scaling procedures. The ground motions with pulse characteristics resulted in smaller forces and moments in the piers due to higher participation of the isolation mode. The scaling procedure had minor influence on the response quantities, expect for pier forces and isolator displacements under near-fault non-pulse ground shaking.

1 INTRODUCTION

India has announced several high-speed railway (HSR) corridors between major cities to meet the mobility needs of the growing population. In general, an HSR network has train speeds that are greater than 200 km/h. Several HSR networks operate around the world, such as China, France, Japan, and Taiwan. India has also announced the first HSR project, which is under construction between the cities of Mumbai and Ahmedabad, which spans over a length of 508 km. The ongoing project primarily involves viaducts with several bridges along the route. Designing HSR bridges in seismic-prone regions poses significant challenges. Currently, the

conventional force-based seismic design is used, which dissipates energy through nonlinear hinge formation in the piers to prevent collapse during earthquakes. However, this approach often requires retrofitting or replacing the damaged regions after an earthquake, incurring downtime and additional costs. Accepting a certain level of risk for structural damage to achieve performance goals (e.g., life safety) is essential for economic design. The performance goals are much more stringent for critical bridges, which need to be operational without damage to assist in post-earthquake recovery and safeguard economic investments. Seismic isolation system can be an effective strategy in mitigating the seismic demands to achieve the performance goals and ensure economic design.

Several highway bridges have been seismically isolated in the past to achieve seismic performance goals (Buckle *et al.*, 2006). Previous studies shows that near-fault ground motions, despite having low PGA compared to far field ground motions, can lead to higher seismic response in isolated bridges (Loh *et al.*, 2002). Near-fault ground motions, with pulse-like velocity form, pose greater destructiveness than peak ground acceleration (Loh, 1999; Makris and Chang, 1998). Seismically isolated bridges with effective period close to the near fault pulse period experiences significant amplification in their responses. This is mainly attributed to the long-period velocity pulse components present in the near-fault ground motions (Shen *et al.*, 2004). Thus it can be concluded from the above studies that, a conventional seismically isolated bridge may experience a higher seismic response against near-fault ground motions.

Further, researches carried out on effect of near-fault ground motions on high-speed rail bridges have been studied. Chen *et al.* (2019) studied the seismic response of both isolated and non-isolated HSR bridges under near-fault ground motions. It has been observed that near-fault ground motions have significant impact on the seismic response of seismically isolated HSR bridges when subjected to a lower A_p/V_p (where, A_p=peak ground acceleration and V_p=peak ground velocity) ratio, with the mean pulse period close to the effective period of the bridge. Thus, similar to conventional bridges long-period seismically isolated bridge may face a low-frequency resonance effect when exposed to a near-fault long-period velocity pulse. This phenomenon can lead to substantial relative pier top displacements in the bridges.

In this paper, the performance of seismically isolated continuous span HSR bridge is assessed subject to near-fault ground motions with pulse and non-pulse characteristics and benchmarked against response to far-fault ground motions for a given seismic hazard. The effect of ground motion scaling procedures on the response of seismic isolated HSR bridges is investigated. The response values are also compared with response limits prescribed by different HSR authorities around the world to determine critical response parameters.

2 DESCRIPTION OF BRIDGE

A benchmark isolated bridge over the Kim River crossing is selected for the current study. A seismic zone IV as per Indian seismic code with medium stiff soil type is assumed for the current study, considering several future corridors are planned in seismic zone IV. The superstructure is a prismatic, prestressed concrete box girder, spanning continuously over three spans, each of length 40 m, as shown in Figure 1. The substructure is composed of two circular piers, each with a height of 18 meters, and abutments at the ends. The superstructure is isolated using eight identical lead rubber bearings (LRB) with two isolator installed at the top of each abutments and piers. Fixed boundary conditions at the base of the piers are assumed to be provided by pile foundations with circular concrete piles. Soil-structure interaction is not considered in the current study.

3 NUMERICAL MODEL

A three-dimensional (3D) finite element (FE) model of the seismically isolated bridge is developed using line elements in SAP2000 (CSI, 2018). Figure 2 (a) and (b) shows the longitudinal section view and cross section view of the numerical model. The deck superstructure is modeled using a generalized section with equivalent

section properties, and it is discretized into small elements, typically 1 meter, along the longitudinal direction. Rigid links, linear elastic beam-column elements with very high stiffness properties, are used to model the rigid offsets between the centroidal axis of the box girder and the isolators. To consider the continuity effect, the rails are explicitly modeled and extend beyond the abutments for a distance of up to 100 m, and additionally, nonlinear boundary springs are installed at the end of the extension (CHSRA, 2014). The rail deck connection springs are used to consider the track structure interaction. The rail deck connection spring is modeled using a multilinear plastic link element consisting of three springs for longitudinal, transverse, and vertical directions. In the longitudinal direction, the connection is modeled as an elastic-perfectly plastic spring with yield deformation of 0.51 mm and initial stiffness of 2.87 kN/mm per meter of track (Li and Conte, 2016). In transverse and vertical directions, the spring is modeled as a linear spring per meter of track (two rails) with a stiffness value of 21.5 kN/mm and 191.5 kN/mm, respectively. The nonlinearity in the pier is introduced by defining the 25 automatic concentrated hinges. Figure 3, shows the 3D FE model of isolated HSR bridge in SAP2000.

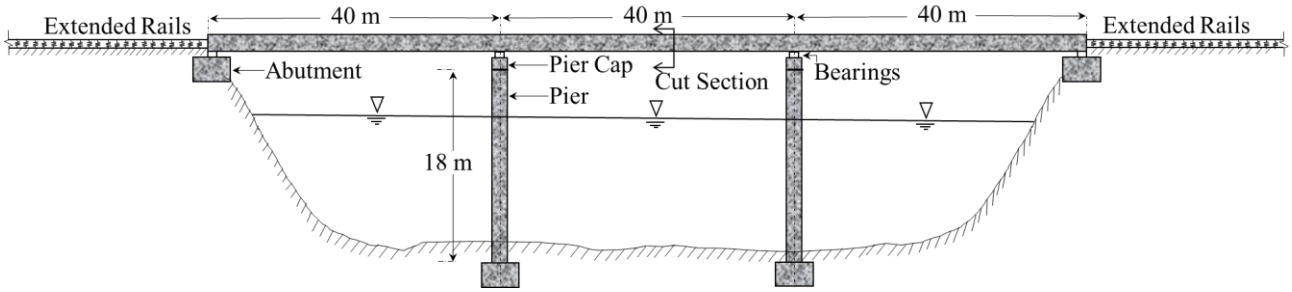

Figure 1: Longitudinal section of the bridge

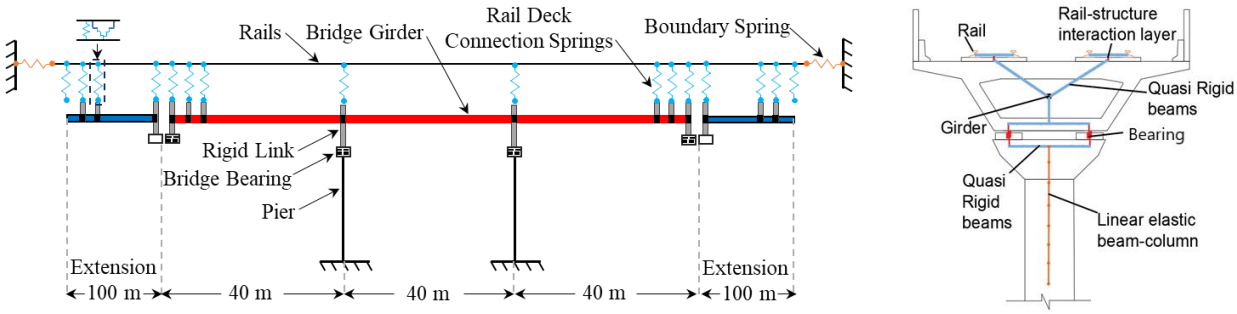

(a) Longitudinal section view *(b) Cross-section view*

Figure 2: Numerical model of benchmark bridge

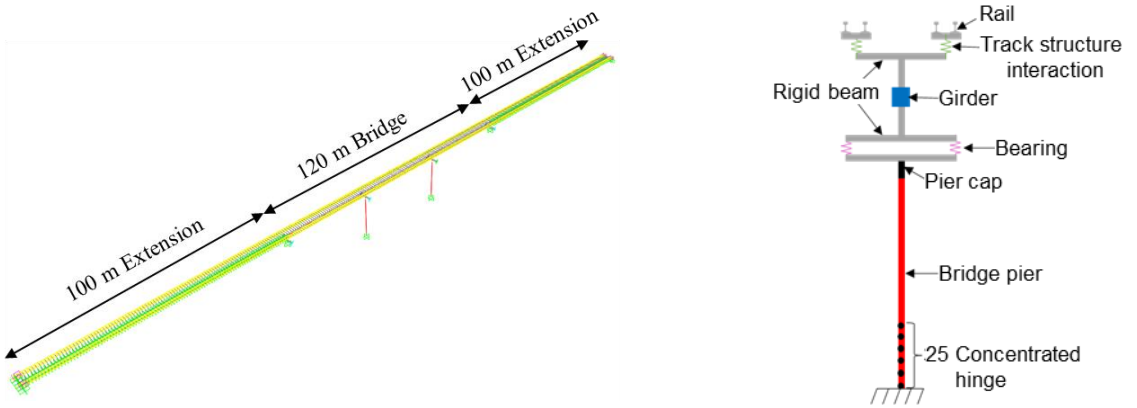

(a) 3D FE model of benchmark HSR bridge *(b) Cross section view of FE model*

Figure 3: Finite element model of benchmark bridge in SAP 2000

3.1 Isolation System

The LRBs are modelled assuming an idealized bilinear inelastic force deformation behaviour in two horizontal directions and rigid in the vertical direction. The minimum lead core diameter is governed by braking and wind loads. The ratio of characteristic strength (Q_d) to the weight of the superstructure (W) for the isolator is considered as 0.087. A total of eight isolators, two isolators at each pier and two isolators at each abutment, are provided with the same mechanical properties. At the abutment, uniaxial isolators are provided to restrain deformation in the transverse direction while complete isolation allowed in the longitudinal direction. The dimensions and the mechanical properties of the isolators are summarized in Table 1.

3.2 Modal Analysis

Modal analysis of the seismically isolated bridge model was performed. The first four mode shapes and their properties are shown in Figure 4. The first and second modes are primarily characterized by deformations in isolators in the transverse (U_y = 65%) and longitudinal (U_x = 80%) directions, respectively. The third and fourth modes are characterized by deformation in the superstructure, which are vertical and rotational modes, respectively.

Table 1: General dimensions and characteristic properties of the isolator.

General dimensions of the isolator		**Characteristic properties of the isolator**	
Lead core diameter	280 mm	Seismic zone	IV
Bonded diameter	900 mm	Q_d/W	0.087
Cover	20 mm	Effective stiffness	8646 kN/m
Steel shim thickness	3 mm – 48 nos.	Yield force	684 kN
Rubber thickness	6 mm – 49 nos.	Elastic stiffness	13162 kN/m
Total height	440 mm	Post-yield stiffness ratio (α)	0.1

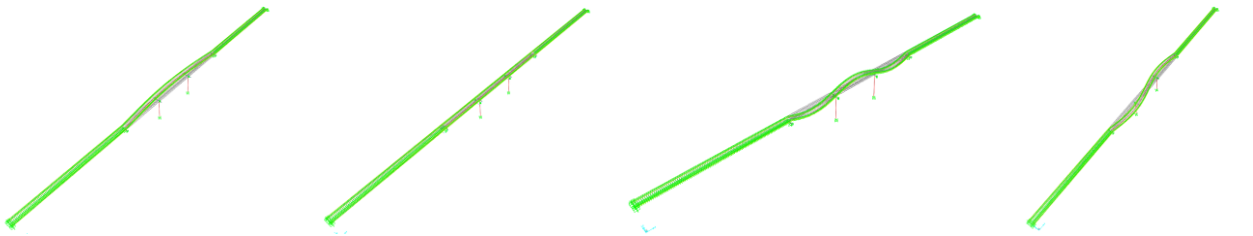

Transverse mode (T = 0.81 sec, U_y = 65%, R_x = 79%)

Longitudinal mode (T = 0.79 sec, U_x = 80%)

Vertical mode (T = 0.29 sec, U_z =7%)

Rotational mode (T = 0.24 sec, R_z=51%)

Figure 4: Modal properties of seismically isolated bridge

4 SEISMIC HAZARD AND GROUND MOTION SCALING

Target spectra for the response history analysis of seismically isolated bridges are defined as per the Indian seismic code IS1893-Part 1 (BIS, 2016), considering seismic zone IV with soil type II (medium stiff) and 5%

damping. The target spectra correspond to the Maximum Considered Earthquake (MCE) hazard level, which is considered two times the design basis earthquake (DBE) as recommend in IS1893-Part 6 (BIS, 2020). This study considers three sets of ground motions representative of three ground shaking scenarios: i) far-fault non-pulse type (FF_NP), ii) near-fault pulse type (NF_P), and iii) near-fault non-pulse type (NF_NP). The complete details of near-fault ground motions and far-fault ground motions are adopted from Pant *et al.* (2013) and Pant and Wijeyewickrema (2013) respectively. Each set contains seven pairs of ground motions, with each pair containing fault normal (FN) and fault parallel (FP) components. These ground motions are scaled to target spectra corresponding to the MCE spectrum, using two scaling procedures: 1) weighted amplitude scaling and 2) spectrum matching.

4.1 Weighted Amplitude Scaling

Weighted amplitude scaling of the three sets of ground motions was performed as per guidelines provided in ASCE 7-16. This process involves scaling the amplitude of ground motion while maintaining the frequency content unchanged. The weighted average scaling process is applied at various time periods: 0.6, 0.7, 0.8, 0.9, 1.0, 1.1, 1.2, and 1.3 sec. For each ground motion, the amplitude is scaled by a factor F_j to minimize the error between the SRSS spectrum of scaled motion and the target MCE spectrum. The factor F_j is determined using Equation 1, where w_i is represents the weightage for i^{th} time period, $S_{MCE}(T_i)$ represents the spectral acceleration at i^{th} time period from MCE spectrum, $S_x(T_i)$ and $S_y(T_i)$ represent the spectral acceleration at the ith time period from the spectrum of both horizontal components (X and Y) of the ground motion.

$$F_j = \frac{\sum_{i=1}^{8} w_i S_{MCE}(T_i)\sqrt{S_x^2(T_i)+S_Y^2(T_i)}}{\sum_{i=1}^{8} w_i\{S_x^2(T_i)+S_Y^2(T_i)\}} \quad (1)$$

To satisfy the ASCE 7 criteria, the average SRSS spectrum of seven ground motions is constructed by multiplying the scaled factor F_j to X and Y components of each ground motion. The average spectrum is then compared with the MCE spectrum in the period range of 0.6 to 1.3 sec. The average spectrum should not be less than MCR spectrum; for this, a scale factor F_1 applies to all ground motions. The final scale factor for each ground motion is the F_jF_1. Finally, the geometric mean spectra are constructed by scaled ground motion, and the average geometric spectra is multiplied by 1.3. This spectrum is compared with 0.9 times the target MCE spectrum in the range of 0.6 to 1.3 sec, to ensure that it does not fall below 0.9 MCE. Figure 5 to Figure 7 shows the comparison of the average SRSS spectrum of scaled ground motions with the MCE spectrum for all three sets of ground motions.

4.2 Spectral Matching

Each set of ground motions was scaled using the SeismoMatch software (Seismomatch, 2016). The scaling period range is selected from 0.5 to 1.5 sec to cover the fundamental time periods of seismically isolated bridge models. Both the fault normal and fault parallel components of the ground motion are scaled to the target spectra using a single scale factor within the specified period range within a scaling tolerance of 10%. The average geomean (GM) spectra of scaled ground motions of all three sets are shown in the Figure 8.

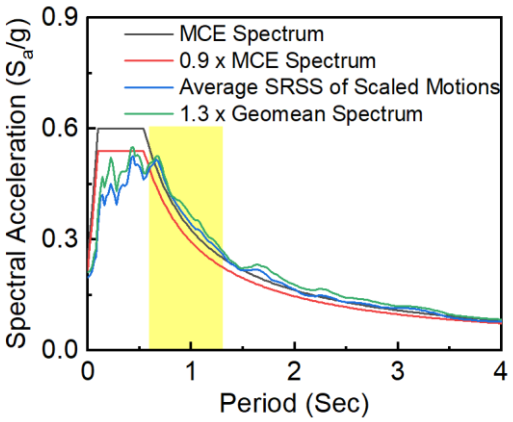

Figure 5: Average SRSS response spectrum of scaled far-fault non-pulse (FF_NP) type ground motions

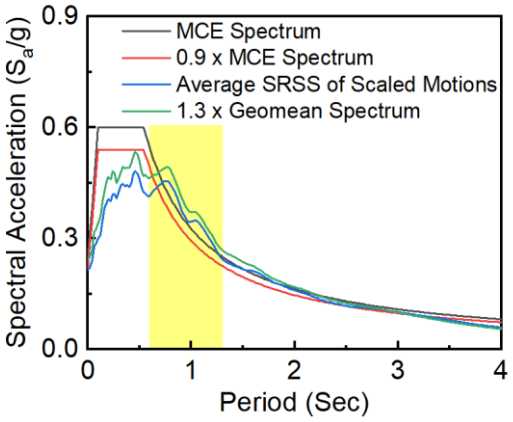

Figure 6: Average SRSS response spectrum of scaled near-fault pulse (NF_P) type ground motions

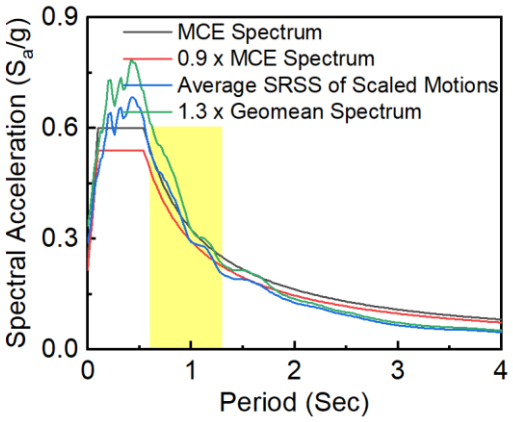

Figure 7: Average SRSS response spectrum of scaled near-fault non-pulse (NF_NP) type ground motions

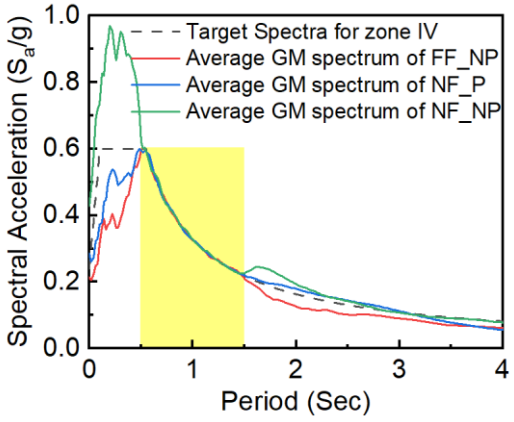

Figure 8: Average GM spectra of scaled ground motions by spectrum matching

5 RESPONSE HISTORY ANALYSIS

Nonlinear response history analysis was performed using SAP2000 for a seismically isolated bridge model subjected to all sets of ground motions and different scaling approaches. The coordinate system of the bridge model is shown in the Figure 9, where the longitudinal direction is along the train running direction, the transverse direction is across the train running direction, and the vertical direction is along the pier height. For analysis, two cases are considered, one with FN along the longitudinal direction and FP along the transverse direction of the bridge, and another with FN along the transverse direction and FP along the longitudinal direction of the bridge. The maximum response from both cases was considered as the overall response for the specific ground motion. Newmark's β-γ method was used, along with 2% Rayleigh damping corresponding to the first and tenth modes. The peak response values considered in this study are the forces at the pier base, displacement at the pier top, mid-span transverse displacement, girder end rotations, deck acceleration, rail stress, and isolator response. The response quantities of seismically isolated bridges are compared subjected to FF_NP ground motion versus NF_P type ground motion versus NF_NP type ground motion for both weightage scaling and spectrum matching.

5.1 Forces and Displacement of the Pier

The normalised forces (F_i) and moments (M_i) were evaluated for weightage scaled ground motions at the base of Pier 2 as shown in Figure 10. The normalization was done by the corresponding response values of far-fault ground motion summarized in Table 2. It is observed that there is no significant difference in the values of F_1

and M_2 (corresponding to longitudinal direction) for near-fault pulse-type ground motion compared to far-fault ground motion. However, there is a significant increment for near-fault non-pulse type ground motion by approximately 60% compared to far-fault ground motion. Similarly, in the transverse direction, F_2 and M_1 are similar for the near-fault pulse type and far-fault type, unlike the near-fault non-pulse type response (40 % higher).

Figure 11 shows the normalised displacement and rotation at the top of Pier 2 for weightage scaled ground motions. The response was normalized by the corresponding response values of far-fault ground motion summarized in Table 2. It is observed that U_1 and R_2 (in longitudinal direction) remain approximately the same for near-fault pulse type compared to far-fault ground motion. However, there is a significant increment for near-fault non-pulse type ground motion by approximately 80% and 60%, respectively compared to far-fault. In the transverse direction, U_2 and R_1 are approximately same for near-fault pulse type where it is approximately 35% higher for near-fault non-pulse type.

5.2 Mid-Span Transverse Deflection and Girder End Rotation

The mid-span transverse deflection and girder end rotations are critical parameters to maintain the track geometry, and both should remain within the limits. Figure 12 shows the mid-span transverse deflection for all three spans corresponding to all three sets of amplitude scaled ground motions. It is observed that the central span (span 2) is more critical than the end span. In a seismically isolated bridge, the deck deflection is increased due to displacement in the isolator. The deck deflection is approximately 12% higher for near-fault pulse-type ground motion compared to far-fault type, whereas it is approximately the same for near-fault non-pulse type to far-fault type. However, these displacements remain within the acceptable limit as provided by California high speed rail authority (CHSRA, 2014).

Figure 13 shows the girder end rotations about the transverse axis (R_2; out-of-plane rotation) and vertical axis (R_3; in-plane rotation) for all three sets of amplitude scaled ground motions at the abutments. It is observed that out-of-plane rotation is the same for all the ground motions, while in-plane rotation is approximately 15% higher for near-fault pulse-type and almost similar for near-fault non-pulse-type compared to far-fault type ground motions, respectively. However, in-plane end rotations exceed the prescribed limits provided by California high speed rail authority (CHSRA, 2014) for all three ground motion sets.

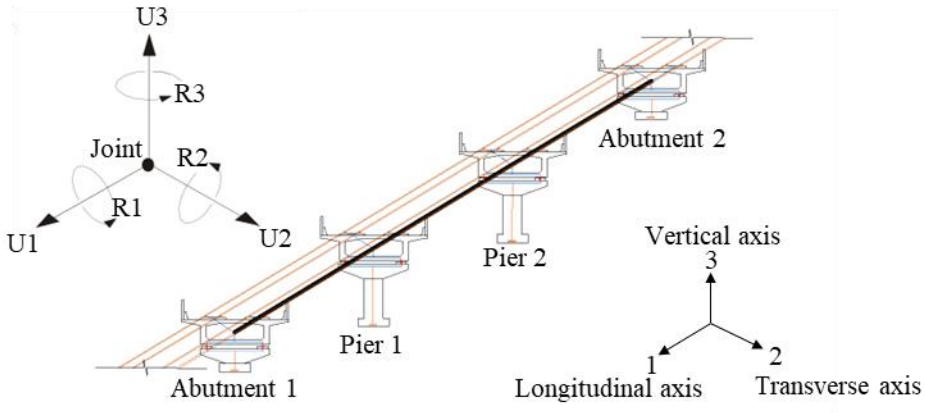

Figure 9: Coordinate system of bridge with degree of freedom

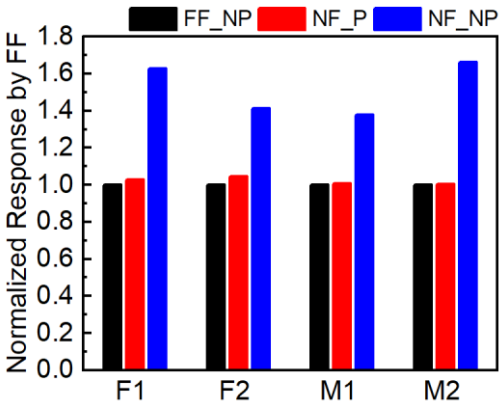

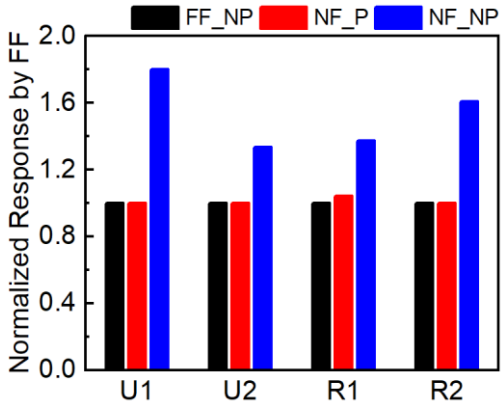

F_i = force along i, M_i = moment about i, U_i = displacement along i, R_i = rotation about i,
[1]Longitudinal direction, [2]Transverse direction

Figure 10: Forces and moments at the pier bottom

Figure 11: Displacement and rotation at pier top

Table 2: Response of isolated bridge in far-fault non-pulse (FF_NP) ground motion

Location	Forces and moments at pier bottom				Displacement and rotation at pier top			
	F_1 (kN)	F_2 (kN)	M_1 (kNm)	M_2 (kNm)	U_1 (mm)	U_2 (mm)	R_1 (deg)	R_2 (deg)
Pier 2	3052	3512	56477	50611	5	6	0.024	0.023

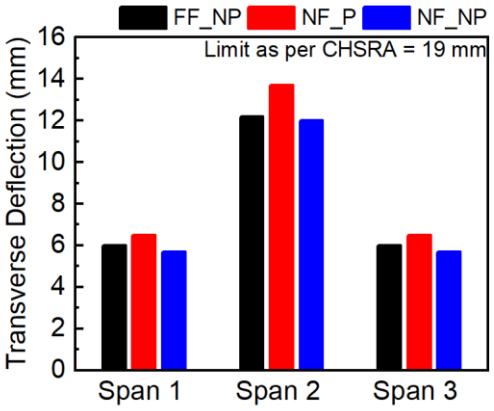

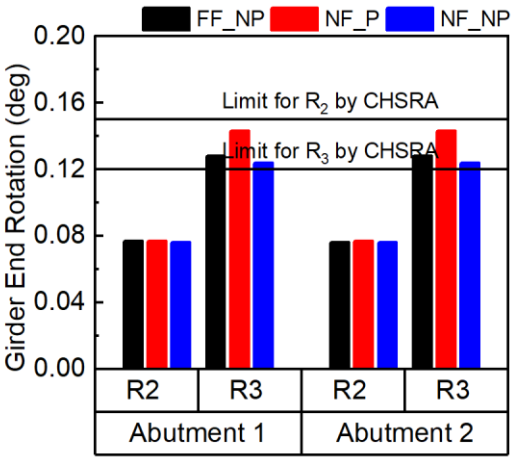

Figure 12: Mid span transverse deflection

Figure 13: Girder end rotation

5.3 Deck Acceleration and Rail Stress

Deck acceleration is important for both track stability and passenger comfort, while rail stress is important from the buckling point of view. Figure 14 shows the deck acceleration in both longitudinal (U_1) and transverse (U_2) directions at various locations, including the mid-span of all spans and above the piers, for all sets of amplitude scaled ground motions. The deck acceleration in the longitudinal directions is lesser compared to the transverse direction at all the locations, as complete isolation is allowed in longitudinal directions. Deck acceleration remains approximately same for all three sets of ground motions. Additionally, the deck

acceleration is lesser than the PGA of the target spectra (0.6g) for all locations except in the transverse direction for the central span.

Figure 15 shows the combined rail stress and additional axial rail stress for all the ground motions. Various combinations of axial stress and bending stress (in transverse and vertical directions) are considered to determine the maximum combined stress. Horizontal lines representing the limits for combined rail stress (factored yield strength 368 MPa) and additional axial rail stress (158 MPa) are included (CHSRA, 2014). It is noted that the combined rail stress and additional axial rail stress for near-fault pulse-type ground motion are approximately 12% higher compared to far-fault type ground motions. However, they remain approximately the same for near-fault non-pulse-type ground motions. Importantly, both stresses exceed the established limits.

5.4 Isolator Response

The mean peak isolator displacements (seven ground motions) for the near and far fault shaking are reported in Table 3. The shear force-displacement loops of an isolator for one of the seven ground motions are plotted in Figure 16. The pulse type near fault ground motions induces higher response in the isolator and thereby resulting in higher participation of the isolation mode. The non-pulse type near and far-fault ground motions provide comparable isolator response. The higher forces and moments in the superstructure for non-pulse type ground motions may be attributed to the lower participation of isolation mode compared to the pulse type ground motion.

5.5 Effect of Scaling

All three sets of ground motions were also scaled using the spectrum matching procedure and the response quantities were calculated and compared against the amplitude scaling in Table 4. There is negligible effect of scaling procedure on the response for far-fault ground motions. The scaling procedure had influence on the response for near fault non-pulse (NF_NP) type ground motion, only for pier forces, deck acceleration and isolator displacements. For the mentioned response quantities, the spectrum matching produced results which were slightly higher than the amplitude scaling. However, in-plane girder end rotation and rail stress for near-fault pulse-type (NF_P) are lesser for spectrum matching. The difference may be attributed to higher transverse deformation in the isolator for amplitude scaled ground motion.

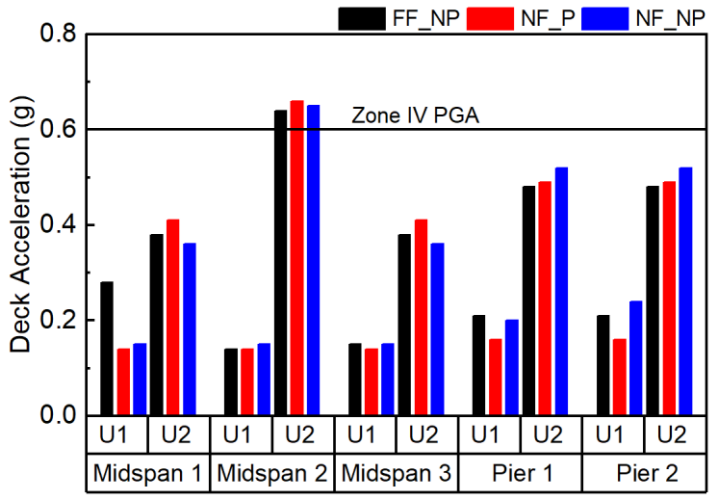

Figure 14: Deck acceleration in longitudinal and transverse directions at different locations

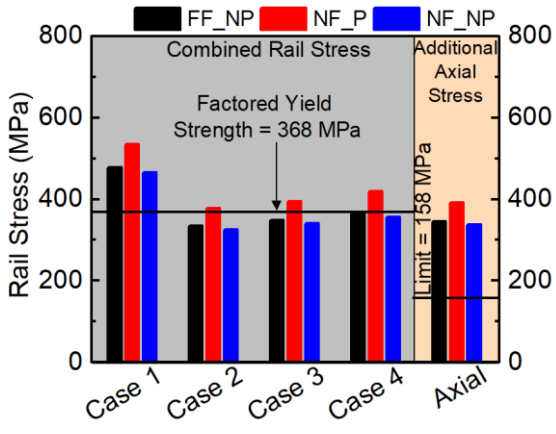

Figure 15: Combined and additional axial rail stress

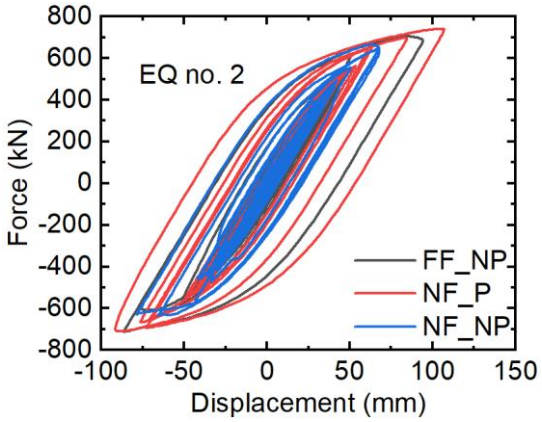

Figure 16: Force deformation curve in transverse direction for pier-2 isolator

Table 3: Mean peak isolator displacements for seven ground motions.

Isolator Deformation (mm)	FF_NP	NF_P	NF_NP
Longitudinal direction	73	79	70
Transverse direction	75	83	73

Table 4: Effect of ground motion scaling procedure on the response of HSR bridge.

Type of Ground motions		FF_NP		NF_P		NF_NP	
Response Quantities		SM	AS	SM	AS	SM	AS
Forces and Moments	F_2 (kN)	4018	3512	4326	3666	8383	4972
	M_1(kNm)	62971	56472	67817	56875	131257	77842
Displacement And Rotation	U_2 (mm)	6	6	7	6	13	8
	R_1 (deg)	0.027	0.024	0.029	0.025	0.055	0.033
Mid-span transverse deflection	Span 2 (mm)	12.3	12.2	12.3	13.7	12.4	12
Girder End Rotation	R_2 (deg)	0.077	0.077	0.077	0.077	0.077	0.076
	R_3 (deg)	0.127	0.128	0.128	0.143	0.128	0.124
Deck Acceleration At mid-span 2	U_1 (g)	0.14	0.14	0.15	0.15	0.18	0.14
	U_2 (g)	0.65	0.64	0.64	0.65	0.95	0.66
Rail Stress	Case 1 (MPa)	478	478	486	534	480	466
	Axial (MPa)	346	346	353	392	348	337
Isolator Deformation	Longitudinal (mm)	76	73	92	79	91	70
	Transverse (mm)	75	75	74	83	78	73

SM = Spectrum matching, AS = Amplitude scaling

6 SUMMARY AND CONCLUSION

This paper discusses the performance of a seismically isolated HSR bridge against near field shaking with and without pulse characteristics and far field ground shaking. Two scaling methodologies, namely, weighted amplitude scaling and spectrum matching, were used to scale the ground motions to match the target spectra defined for Zone IV of Indian seismic code. A three-dimensional nonlinear FE model of the seismically isolated HSR bridge was developed to assess its performance under all sets of scaled ground motions. The response of the bridge was compared with the limits set by existing HSR bridge projects for safety and serviceability. It was observed that seismic demands were higher for near-fault ground motions, especially in the non-pulse type category, compared to far-fault ground motions. This may be due to the lower participation of the isolation modes in near-fault non-pulse type ground motion. Other critical response parameters such as transverse deflection, girder end rotation, and rail stress were also studied. Near-fault pulse type motions showed higher values for these parameters compared to far-fault and near-fault non-pulse type motions, although they remained within acceptable limits for all three sets of ground motions except for rail stress, which exceeded the limits. Isolator deformation was higher in near-fault pulse type motions compared to far-fault non-pulse type and near-fault non-pulse type motions. The seismic demand, deck acceleration, and isolator deformation are slightly higher for spectrum matching compared to amplitude scaling. The other response parameters remained approximately same for spectrum matching compared to amplitude scaling. Isolator deformation was higher for near-fault ground motions, both pulse and non-pulse types, compared to far-fault motions in the longitudinal direction, possibly due to complete isolation being allowed in this direction.

Overall, near-fault non-pulse type ground motions induced more severe effect compared to near-fault pulse type and far-fault non-pulse type motions. Additionally, spectrum matching showed higher seismic demand than amplitude scaling, especially for near-fault non-pulse type motions. The critical parameters, such as mid-span transverse deflection and girder end rotations, are within the limit, but rail stresses exceeding the limit. The rail stress can be controlled by using a higher Q_d/W ratio, or the isolator design can be governed by rail stresses rather than braking loads.

REFERENCE

BIS (2016). "Criteria for Earthquake Resistant Design of Structures, Part 1: General provisions and buildings." *Standard IS 1893, Rev 6*, Bureau of Indian Standards, New Delhi, India.

BIS (2020). "Criteria for Earthquake Resistant Design of Structures, Part 6: Base Isolated Buildings." *IS 1893*, Bureau of Indian Standards, New Delhi, India.

Buckle, I. G., Constantinou, M., Dicleli, M., and Ghasemi, H. (2006). "Seismic Isolation of Highway Bridges." Report Technical Report MCEER-06-SP07, University at Buffalo, State University of New York, Buffalo, NY.

Chen, L.-k., Jiang, L.-z., Qin, H.-x., Zhang, N., Ling, L., Zhang, Q.-h., Li, Q., and Cao, D.-f. (2019). "Nonlinear seismic assessment of isolated high-speed railway bridge subjected to near-fault earthquake scenarios." *Structure Infrastructure Engineering*, 15(11), 1529-1547.

CHSRA (2014). "Track-Structure Interaction." *TM 2.10.10*, California High-Speed Rail Authority, California, USA.

Computer & Structures Inc. (CSI) (2018). Computer Program SAP2000, Berkeley, CA.

Li, Y., and Conte, J. P. (2016). "Effects of seismic isolation on the seismic response of a California high‐speed rail prototype bridge with soil‐structure and track‐structure interactions." *Earthquake Engineering & Structural Dynamics*, 45(15), 2415-2434.

Loh, C.-H., Liao, W.-I., and Chai, J.-F. (2002). "Effect of near-fault earthquake on bridges: lessons learned from Chi-Chi earthquake." *Earthquake Engineering Vibration*, 1, 86-93.

Loh, C. (1999). "Interpretation of structural damage in 921 Chi-Chi-earthquake." *Proceedings: Proceedings of international workshop on Chi-Chi, Taiwan earthquake of September*, 14-17.

Makris, N., and Chang, S. P. (1998). "Effect of damping mechanisms on the response of seismically isolated structures."Pacific Earthquake Engineering Research Center Berkeley, CA, USA.

Pant, D. R., Constantinou, M. C., and Wijeyewickrema, A. C. (2013). "Re-evaluation of equivalent lateral force procedure for prediction of displacement demand in seismically isolated structures." *Engineering Structures*, 52, 455-465.

Pant, D. R., and Wijeyewickrema, A. C. (2013). "Influence of near-fault ground motions on the response of base-isolated reinforced concrete buildings considering seismic pounding." *Advances in Structural Engineering*, 16(12), 1973-1988.

Seismosoft (Seismomatch) (2016). Computer Program A computer program for spectrum matching of earthquake records.

Shen, J., Tsai, M.-H., Chang, K.-C., and Lee, G. C. (2004). "Performance of a seismically isolated bridge under near-fault earthquake ground motions." *Journal of Structural Engineering*, 130(6), 861-868.